ELSEVIER

Nuclear Instruments and Methods in Physics Research A 412 (1998) 1–18

NUCLEAR INSTRUMENTS & METHODS IN PHYSICS RESEARCH Section A

A Fabry–Pérot cavity for Compton polarimetry

J.P. Jorda[a], E. Burtin[a], Ch. Cavata[a,*], J. Jardillier[a], B. Frois[a], D. Neyret[a], J. Martino[a], S. Platchkov[a], T. Pussieux[a], M. Authier[a], P. Deck[a], N. Falletto[a], J.C. Sellier[a], C. Veyssière[a], A. Delbart[a], Ph. Mangeot[a], Ph. Rebourgeard[a], N. Colombel[a], P. Girardot[a], G. Zavattini[b]

[a] *DAPNIA CEA Saclay, 91191 Gif/Yvette Cedex, France*
[b] *INFN, Via Paradiso, 12, I-44100 Ferrara, Italy*

Received 25 November 1997

Abstract

A new kind of Compton polarimeter using a resonant Fabry–Pérot cavity as a power buildup for the photon beam is proposed. A prototype of such a cavity is described, along with the results obtained in terms of source to be used in a Compton scattering polarimeter.

1. Introduction

To carry the ambitious Physics program at Jefferson Lab with polarized electrons [1], a precise measurement of the electron beam polarization is required in the 1–10 GeV energy range for currents between 1 and 100 μA.

At these energies, a well-known technique is to use Møller scattering [2,3]. However, during such a beam polarization measurement the experimental data taking is stopped, thus preventing a continuous monitoring. Another major problem is that Møller polarimeters can only be used at low intensity beam (typically 10 μA) and experiments have to assume that beam polarization remains constant when the intensity of the beam is one order of magnitude higher.

An alternate, widely used technique at high energy [4–9], is Compton scattering. The longitudinal polarization is extracted from the measurement of the counting rate asymmetry for opposite electron helicities in the scattering of a circularly polarized photon beam on the electron beam. A precision of 0.7% has been achieved at SLAC using this method [8,9]. In the Jefferson Lab. energy range, such a polarimeter has a relatively low figure of merit.

In this paper, we present a new type of Compton polarimeter based on a resonant Fabry–Pérot cavity as a power buildup for the photon beam. We first show that for Jefferson Lab. (TJNAF) conditions, the use of a standard 1W Laser does not allow a rapid and precise monitoring of the polarization. The principle of a Fabry–Pérot cavity used as a power buildup for the photon density is then

* Corresponding author. Tel.: + 33 1 69 08 2637; fax: + 33 1 69 08 7584; e-mail: ccavata@cea.fr.

0168-9002/98/$19.00
PII: S0168-9002(98)00226-5

explained. The results obtained at Saclay with a Fabry–Pérot cavity prototype are given. As a conclusion, the expected difficulties to install such a cavity at Jefferson Lab. are discussed.

2. Principle of the method

With a Compton scattering polarimeter, the longitudinal polarization P_e of the electron beam is determined using the measurement of the counting rate asymmetry in Compton scattering with circularly polarized light (polarization P_γ)

$$A_{exp} = \frac{n^+ - n^-}{n^+ + n^-} = P_e P_\gamma A_\ell. \quad (1)$$

n^+ (resp. n^-) is the number of Compton scattering events before (resp. after) a reversal of the electron polarization ($P_e \to -P_e$). This experimental asymmetry is related to the known theoretical asymmetry A_ℓ for Compton scattering of electron and photon with spin parallel $\sigma^{\rightarrow}_{\Rightarrow}$ and anti-parallel $\sigma^{\leftarrow}_{\Rightarrow}$,

$$A_\ell = \frac{\sigma^{\rightarrow}_{\Rightarrow} - \sigma^{\leftarrow}_{\Rightarrow}}{\sigma^{\rightarrow}_{\Rightarrow} + \sigma^{\leftarrow}_{\Rightarrow}}. \quad (2)$$

A_{exp} and P_γ are measured quantities and A_ℓ is calculated in the framework of the standard model so that the only remaining unknown quantity is the electron beam longitudinal polarization P_e.

The rates of Compton scattering $dn^\pm/dt$ depend on the luminosity $\mathscr{L}^\pm$, the unpolarized cross-section for Compton scattering $\sigma_0 = \frac{1}{2}(\sigma^{\rightarrow}_{\Rightarrow} + \sigma^{\leftarrow}_{\Rightarrow})$ and the polarization of the electron and photon beams

$$\frac{dn^\pm}{dt} = \mathscr{L}^\pm \sigma_0 [1 \pm P_e P_\gamma A_\ell]. \quad (3)$$

The photon source is a Laser, providing photons with energy around $k = 2\,\text{eV}$ for visible light.

The collision with the electron beam is almost a head-on collision (very small crossing angle, $\alpha_c \simeq 20\,\text{mrad}$) in order to maximize the interaction length and the energy of the back-scattered photons. The maximum back-scattered photon energy is given by $k'_{max} \simeq 4k(E^2/m^2)/(1 + 4kE/m^2)$. For a green Laser (with wavelength $\lambda = 532\,\text{nm}$) the maximum energy of the back-scattered photons is $k'_{max} = 500\,\text{MeV}$.

At zero crossing angle the differential unpolarized cross-section (Fig. 1) is [10,11]

$$\frac{d\sigma_0}{d\rho} = 2\pi r_0^2 a \left[1 + \frac{\rho^2(1-a)^2}{1-\rho(1-a)} + \left(\frac{1-\rho(1+a)}{1-\rho(1-a)} \right)^2 \right], \quad a = \frac{1}{1+4kE/m^2}, \quad (4)$$

where r_0 is the classical radius of the electron and $\rho = k'/k'_{max}$ is the scattered photon energy

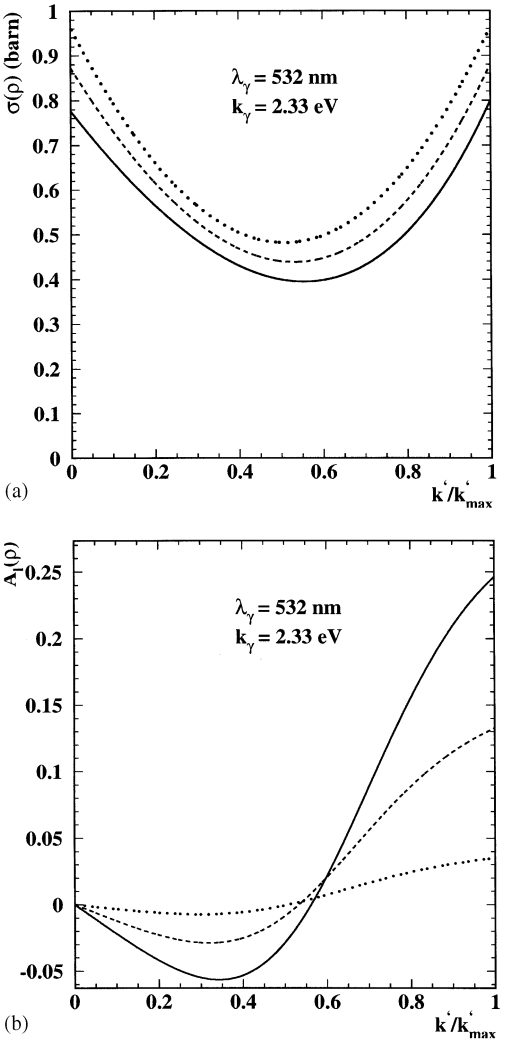

Fig. 1. Cross-section and longitudinal differential asymmetry for 1, 4, 8 GeV beam energy (dotted, dashed, solid line).

normalized to its maximum. At 4 GeV, the total Compton cross section is $\sigma_t = 0.585$ barn for a green Laser.

The longitudinal differential asymmetry (Fig. 1) is given by [10,11]

$$A_\ell = \frac{d\sigma^{\rightarrow}_{\Rightarrow}/d\rho - (d\sigma^{\leftarrow}_{\Rightarrow}/d\rho)}{d\sigma^{\rightarrow}_{\Rightarrow}/d\rho + (d\sigma^{\leftarrow}_{\Rightarrow}/d\rho)} = \frac{2\pi r_0^2 a}{d\sigma_0/d\rho}(1-\rho(1+a)) \times\left[1-\frac{1}{(1-\rho(1-a))^2}\right]. \quad (5)$$

When this asymmetry is measured as a function of the scattered photon energy, the time T needed to achieve a statistical accuracy σ_{P_e} on the electron polarization is given by $T^{-1} = \mathscr{L}(\sigma P_e/P_e)^2 P_e^2 P_\gamma^2 \sigma_t \langle A_\ell^2\rangle$, where

$$\langle A_\ell^2\rangle = \frac{\int_0^1 d\rho\,(d\sigma_0/d\rho)(\rho) A_\ell^2(\rho)}{\int_0^1 d\rho\,(d\sigma_0/d\rho)(\rho)}.$$

At 4 GeV, this asymmetry is $\sqrt{\langle A_\ell^2\rangle} \simeq 6.4\%$ for a green laser.

At TJNAF, the emittance of the electron beam is negligible ($\simeq 10^{-9}$ mrad) and the focalization at the Compton Interaction Point (IP) will be $\sigma_e \simeq 100\,\mu$m. A standard laser can deliver beam with a divergence and size at the Compton IP close to $\varepsilon_\gamma \simeq 1$ mrad and $\sigma_\gamma \simeq 200\,\mu$m. Under these conditions, the angular divergences of the electron and Laser beams are small with respect to the crossing angle α_c, and the differential luminosity along the beam direction z ($z = 0$ at the Compton IP) is given by

$$\frac{d\mathscr{L}}{dz} \simeq c(1+\cos(\alpha_c))\frac{N_{0e}N_{0\gamma}}{2\pi} \times \frac{1}{\sigma_e^2+\sigma_\gamma^2}\exp\left(-\frac{2z^2\sin^2(\alpha_c/2)}{\sigma_e^2+\sigma_\gamma^2}\right), \quad (6)$$

where the normalization factors N_{0e} and $N_{0\gamma}$ are functions of the electron beam current I_e and Laser power P_L

$$N_{0e} = \frac{I_e}{ec} \quad \text{and} \quad N_{0\gamma} = \frac{P_L\lambda}{hc^2}.$$

The differential luminosity distribution is thus Gaussian, so that one can define a $\pm 1\sigma$ interaction length by $L^{int} \simeq 2\sqrt{\sigma_e^2+\sigma_\gamma^2}/\sin(\alpha_c)$. Integrating Eq. (6) yields the total luminosity

$$\mathscr{L} \simeq \frac{(1+\cos(\alpha_c))}{\sqrt{2\pi}}\frac{I_e}{e}\frac{P_L\lambda}{hc^2}\frac{1}{\sqrt{\sigma_e^2+\sigma_\gamma^2}}\frac{1}{\sin(\alpha_c)}. \quad (7)$$

For a green Laser, with power $P_L = 1$ W, this gives for an electron beam current $I_e = 100\,\mu$A a luminosity of $\mathscr{L} \simeq 100\,\text{barn}^{-1}\,\text{s}^{-1}$ and an interaction length of $L^{int} \simeq 2$ cm. Under these conditions, a measurement of a beam polarization $P_e = 50\%$ at the 1% statistical level is done within 2 days.

In order to be able to measure the polarization at lower current and more rapidly to monitor the polarization as necessary for very precise experiments such as Parity violation experiments [12,13], the luminosity of the Compton polarimeter will be enhanced by using a high finesse Fabry–Pérot cavity.

The idea is to trap the laser beam inside a resonant cavity consisting of two high reflectivity mirrors, so that at resonance the power circulating inside the cavity (and seen by the electron beam, see Fig. 2) is enhanced by a factor $\mathscr{G}_0$, the build up coefficient, with respect to the laser power. Cavity gain on the order of 1000 and power density of 1 MW cm^{-2} can be obtained.

3. Basics of a Fabry–Pérot cavity

3.1. Gaussian beam and Fabry–Pérot cavity

The Laser used to feed the cavity delivers a Gaussian beam. The complex electric field of a Gaussian beam propagating along the z-direction at pulsation ω, in a medium of refractive index $n = kc/\omega$, at a wavelength $\lambda = 2\pi/k = \lambda_0/n$ is given by [14,15]

$$E(\boldsymbol{r}, t)_{mp} = E_0\frac{d_0}{d(z)}e^{-i(kz-\omega t)}e^{i(m+p+1)\Psi(z)} \times e^{-ik(x^2+y^2)/2R^2(z)} \times e^{-(x^2+y^2)/d^2(z)} \times H_m\left(\frac{\sqrt{2}x}{d(z)}\right)H_p\left(\frac{\sqrt{2}y}{d(z)}\right).$$

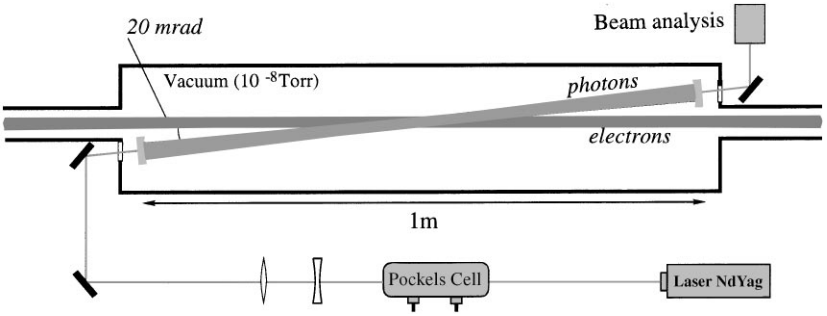

Fig. 2. Principle of Compton Polarimetry with a Fabry–Pérot cavity.

The waist beam spot size d_0 is related to the Rayleigh range z_R, by $d_0^2 = (\lambda/\pi)z_R$. The beam size $d(z)$, the phase $\Psi(z)$ and the wave radius of curvature $R(z)$ evolve along the z-axis according to

$$d(z) = 2\sigma_\gamma(z) = d_0\sqrt{1 + z^2/z_R^2}, \quad \Psi(z) = \tan^{-1}\frac{z}{z_R},$$
$$R(z) = z\left(1 + \frac{z_R^2}{z^2}\right). \tag{8}$$

H_m and H_p are Hermite polynomials and m,p are two integers that define the *transverse mode* of the Gaussian beam. The highest photon density is obtained for the fundamental mode ($p = m = 0$).

When a Gaussian beam is trapped in a resonator consisting of two identical mirrors with radius of curvature R_M separated by a distance L, a perfect mode matching is ensured if $R(z = \pm L/2) = \pm R_M$. Defining $g = 1 - L/R_M$, the cavity parameter, the Rayleigh range, the beam waist size and the diameters of the beam on each mirror for a beam in a resonant symmetric cavity are

$$z_R = \frac{L}{2}\sqrt{(1+g)/(1-g)}, \quad d_0^2 = \frac{\lambda}{\pi}\frac{L}{2}\sqrt{(1+g)/(1-g)},$$
$$d_1^2 = d_2^2 = \frac{2d_0^2}{1+g}. \tag{9}$$

The stability of the resonator requires that $-1 \leqslant g \leqslant 1$, and the waist size decreases as $g \to -1$.

For a transverse mode defined by m and p, the allowed *longitudinal modes* have resonant pulsations given by

$$\omega_\ell(mp) = \Delta\omega_{FSR}\left(l + \frac{1}{\pi}(m + p + 1)\cos^{-1}\sqrt{g^2}\right),$$
$$l = 0,1,\ldots, \tag{10}$$

where $\Delta\omega_{FSR} = 2\pi c/2L = 2\pi\,\Delta\nu_{FSR}$ is the free spectral range (FSR) of the cavity.

3.2. High reflectivity dielectric mirrors

To allow light to perform a maximum number of round trips in the cavity, high reflectivity and low loss mirrors must be used. Mirrors with high reflectivity are obtained through the design of multi-layer quarter-wave dielectric film. Indeed, it can be shown [16] that, at normal incidence, for a mirror with a multi-layer structure of N pairs of layers with index and thickness n_2, h_2 and n_3, h_3, with $n_2h_2 = n_3h_3 = \lambda_0/4$, the reflectivity is

$$R_{2n} = \left(\frac{1 - \frac{n_l}{n_1}\left(\frac{n_2}{n_3}\right)^{2N}}{1 + \frac{n_l}{n_1}\left(\frac{n_2}{n_3}\right)^{2N}}\right)^2, \tag{11}$$

where n_1 (resp. n_l) is the index of the material before the multi-layers (resp. the index of the substrate). For instance, with 14 pairs of Ta_2O_5 ($n_2 = 2.1$), SiO_2 ($n_3 = 1.47$) $\lambda/4$ layers deposited on a SiO_2 substrate, the reflectivity is $1 - R \simeq 100$ ppm.

3.3. Gain in a Fabry–Pérot cavity

We consider a symmetric cavity with two identical mirrors M_1 and M_2 with transmissivity and reflection coefficients t, r, separated by a distance L.

The reflection r and transmissivity t coefficients of the mirrors are defined by $r = E_R/E_I$, $t = E_T/E_I$, where E_I, E_R and E_T are the electric fields of the incident, reflected and transmitted light. In terms of energy, we define the reflectivity R and the transmissivity T of a mirror by $R = J_R/J_I$, $T = J_T/J_I$, where J_k ($k = I, R, T$), the amount of energy per unit area per second, is proportional to $|E_k|^2$. At normal incidence, relations $R = |r|^2$, $T = |t|^2$ apply. In steady state, the field circulating in the cavity E_{circ} is related to the incident field by E_I by [15]

$$\frac{E_{circ}}{E_I} = \frac{it}{1 - r^2 e^{-\delta_0/2} e^{-i2L\omega/c}}. \tag{12}$$

Here δ_0 represents the round trip energy absorption of the cavity medium. In terms of intensity, this gives for the cavity gain $\mathcal{G} = I_{circ}/I_I$ (at normal incidence):

$$\mathcal{G}(\omega) = \mathcal{G}_0 \frac{1}{1 + (2\mathcal{F}/\pi)^2 \sin^2(\pi\omega/\Delta\omega_{FSR})} \quad \text{where}$$

$$\frac{\mathcal{F}}{\pi} = \frac{\sqrt{R e^{-\delta_0/2}}}{1 - R e^{-\delta_0/2}} \tag{13}$$

is the finesse of the cavity. For frequencies that are multiple of the FSR, $\omega_l = l\Delta\omega_{FSR}$, the cavity has maximum gain $\mathcal{G}_0$:

$$\mathcal{G}_0 = \frac{T}{(1 - R e^{-\delta_0/2})^2} = \frac{1 - R - P}{(1 - R e^{-\delta_0/2})^2}, \tag{14}$$

where the energy conservation for the reflection on a mirror with transmissivity T, reflectivity R and total loss P, $1 = T + R + P$ was used.

The bandwidth $\Delta\omega_{cav}$ of the cavity is the FWHM of the frequency response of the cavity gain (Eq. (13)) and is related to the finesse by

$$\frac{\Delta\omega_{cav}}{\Delta\omega_{FSR}} = \frac{\Delta\nu_{cav}}{\Delta\nu_{FSR}} = \frac{2}{\pi} \sin^{-1}\left(\frac{\pi}{2\mathcal{F}}\right) \simeq \frac{1}{\mathcal{F}}. \tag{15}$$

The approximation is valid for a high finesse cavity.

For a symmetric 80 cm cavity made of two mirrors with $R = 99.99\%$, $P = 5$ ppm, the FSR is $\Delta\nu_{FSR} = 187$ MHz, the cavity bandwidth is $\Delta\nu_{cav} = 6$ kHz, the finesse is $\mathcal{F} = 31\,000$ and the maximum gain is $\mathcal{G}_0 = 9500$. Whereas for a symmetric 80 cm cavity made of two mirrors with $R = 99.8\%$, $P = 700$ ppm, the FSR is $\Delta\nu_{FSR} = 187$ MHz, the cavity bandwidth is $\Delta\nu_{cav} = 119$ kHz, the finesse is $\mathcal{F} = 1570$ and the maximum gain is $\mathcal{G}_0 = 325$ (Fig. 3).

3.4. Field reflected by the cavity

The feedback system between the laser and the cavity (see Section 4) is based on the analysis of the phase of the reflected field E_R [17–19]. If ε is the detuning parameter, i.e. the difference between the laser pulsation ω and the nearest resonance frequency of the cavity $\omega_c = n\Delta\omega_{FSR}$ in FSR units, $\varepsilon = (\omega - \omega_c)/\Delta\omega_{FSR}$, then for a medium without absorption, the reflection coefficient ρ of the cavity is

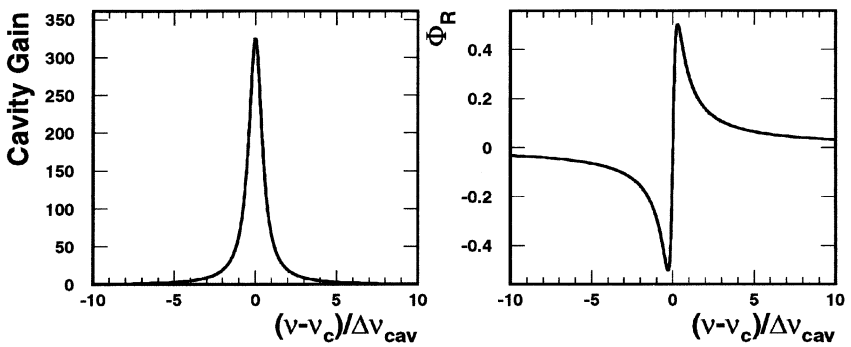

Fig. 3. Cavity gain $\mathcal{G}$, and phase Φ_R of a 80 cm symmetric cavity, with identical mirrors with a reflectivity $R = 99.8\%$ and total loss $P = 700$ ppm, allowing a maximum gain of 325, with a bandwidth of 120 kHz.

given by [15]

$$\rho = \frac{E_R}{E_I} = r\left[\frac{1-(r^2+t^2)\,e^{-2i\pi\varepsilon}}{1-r^2\,e^{-2i\pi\varepsilon}}\right]. \quad (16)$$

The cavity reflectivity $\mathscr{R} = |\rho|^2$ is thus

$$\mathscr{R}(\varepsilon) = \mathscr{R}_0 \frac{1+\frac{4(1-P)}{P^2}\sin^2\pi\varepsilon}{1+(\frac{2\mathscr{F}}{\pi})^2\sin^2\pi\varepsilon}, \quad \text{with}$$

$$\mathscr{R}_0 = R\left[\frac{P^2}{(1-R)^2}\right]. \quad (17)$$

The phase Φ_R of the reflection coefficient $\rho = \sqrt{\mathscr{R}}\,e^{i\Phi_R}$, is given by

$$\tan\Phi_R(\varepsilon) = \frac{(1-P-R)\sin 2\pi\varepsilon}{1-(1-P-R)\cos 2\pi\varepsilon + R(1-p)}$$

$$\simeq 2\pi\varepsilon\left\{\frac{1-R-P}{P(1-R)}\right\}. \quad (18)$$

For small detuning parameter, the phase of the reflected field is proportional to the detuning parameter, and varies very rapidly around a resonance (Fig. 3), so that a measurement of this phase may be used to correct for detuning. This is the key idea of the Pound–Drever method used for the cavity feedback system.

4. Feedback control of the laser frequency

The maximum gain is obtained when the detuning parameter vanishes. Due to thermal and mechanical noises, drift and jitter of the laser, both the laser frequency and the cavity resonance frequencies vary with time, so that the resonance condition for a cavity with a narrow resonance peak (i.e. high gain) is almost never achieved. The feedback control system aims to adapt the laser frequency in order to get $\varepsilon = 0$ with a dispersion as small as possible. The most suitable method is the Pound–Drever locking technique, which has been used successfully in several experiments using a Fabry–Pérot cavity [17–21].

Around resonance Φ_R is proportional to the detuning parameter (Eq. (18)) and thus may be used as discriminator signal (DS). There is no direct way to measure this phase. To build the DS, the laser light (at pulsation ω) is phase modulated with a pulsation $\Omega = 2\pi\nu_\Omega$ and the intensity of the beam reflected by the cavity is measured and demodulated (Fig. 4)

For a small phase modulation with amplitude $\beta \ll 1$, the incident electric field of the Laser

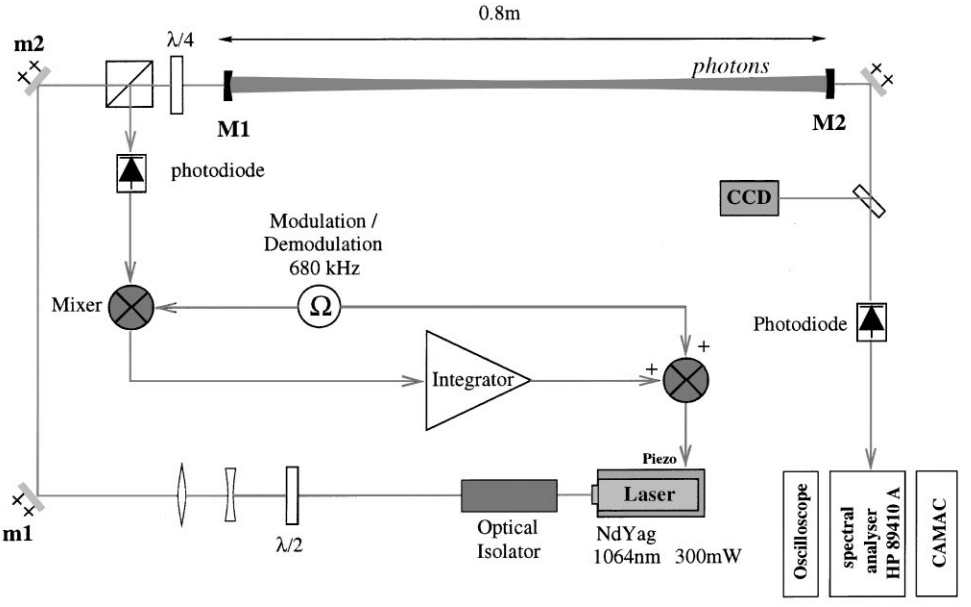

Fig. 4. Setup for the prototype, with feedback control of the laser frequency.

light is

$$E_I = E_0\, e^{i\omega t}\, e^{i\beta\cos(\Omega t+\Phi_\Omega)} \simeq E_0\,(J_0(\beta)\, e^{i\omega t} + iJ_1(\beta)[e^{i(\omega+\Omega)t} + e^{i(\omega-\Omega)t}]). \quad (19)$$

This is a three-term sum of pulsations ω, $\omega+\Omega$, $\Omega-\omega$, whose amplitudes are given by the first Bessel functions $J_{0,1}(\beta)$. Each term is reflected by the cavity with different reflection coefficients $\rho(\omega)$, $\rho(\omega+\Omega)$, $\rho(\omega-\Omega)$:

$$E_R = E_0 J_0 \rho(\omega) e^{i\omega t} + iE_0 J_1[\,\rho(\omega+\Omega)\, e^{i(\omega+\Omega)t} + \rho(\omega-\Omega)\, e^{i(\omega-\Omega)t}\,]. \quad (20)$$

The intensity of the light reflected by the cavity contains several components. For a modulation frequency in the range $\Delta\omega_{FSR} \ll \Omega \ll \Delta\omega_{cav}$ the term which is modulated at pulsation Ω is proportional to $\sin(\Phi_R)$:

$$I_\Omega = 4E_0^2 J_0(\beta)J_1(\beta)|\rho(\omega)|^2 \cos(\Omega t)\sin(\Phi_R). \quad (21)$$

To obtain the DS, the reflected light is detected by a fast photodiode (PD). The PD signal after demodulation and filtering of the high frequencies (above the frequency of the modulation) provides the DS voltage:

$$V_{PD} \simeq \kappa E_0^2 J_0(\beta)J_1(\beta)|\rho(\omega)|^2 \sin(\Phi_R), \quad (22)$$

where κ stands for several electronic and optical parameters. After appropriate electronic filtering and amplification, this DS is sent to an actuator to adapt the laser frequency (Fig. 4).

5. Prototype of the Fabry–Pérot cavity

A prototype of a Fabry–Pérot cavity has been built at Saclay. It is used to elaborate the feedback system for the laser frequency control, to test optical alignment procedures and to define the mechanical drawing of the cavity.

5.1. Description of the prototype

5.1.1. The Nd : YAG laser

The choice of the laser is a compromise between several requirements: high power, short wavelength (to get a high Compton asymmetry), reliability, large wavelength (for which quarter-wave multilayer dielectric mirrors are easier to build).

We have selected the LightWave Series 126 Nd : YAG laser operating at 1064 nm. It is a diode-pumped solid-state non-planar ring laser, that delivers up to 300 mW CW of single unidirectional longitudinal mode TEM_{00}, with a narrow linewidth (5 kHz over 1 ms). The LightWave Series 126 laser has a noise reduction system that guarantees a noise amplitude smaller than 0.02% over the range from 10 Hz to 2 MHz. The frequency jitter and drift of the laser are respectively $75\,kHz\,s^{-1}$ and $50\,MHz\,h^{-1}$. This laser is easy to use and frequency tunable. There are two ways to tune the laser frequency. The first one is a SLOW frequency tuning that affects the temperature of the Nd : YAG crystal. This allows a tuning range of tens of GHz with relatively slow time constant (1–10 s). Its tuning coefficient, K_S, is $1.6\,GHz\,V^{-1}$ in a 1–10 V voltage range. The second one is a FAST frequency tuning. By applying a voltage to a piezoelectric bounded onto the crystal, the frequency of the laser can vary by tens of MHz at a rate up to 30 kHz. The tuning coefficient K_F, is around $3.2\,MHz\,V^{-1}$. The piezoelectric can operate at higher frequency but the tuning coefficient is different. It can be modeled as a first order system with cut-off frequency $f_{cut}^F \simeq 50\,kHz$.

5.1.2. The optical layout

The setup of the prototype is described in Figs. 4–6. The nonconfocal Fabry–Pérot cavity consists of two high reflectivity (up to 99%) concave ($R_M = 50$ cm, 1 in. diameter) mirrors (M_1 and M_2). These are TECHOPTIC mirrors (Ref. B1051.188.000), with 14 pairs of layers of ZrO_2 and SiO_2, distributed by MELLES GRIOT. The main optical characteristics of the optical setup are summarized in Table 1. The maker specifications for these mirrors are a reflectivity $R > 99.7\%$ and a maximum power density of $> 1\,MW\,cm^{-2}$. Using a LABMASTER ULTIMA power-meter from COHERENT, with detector heads LM2 and LM3 (5% accuracy), the transmissivity of our mirrors was measured to be $T = 700 \pm 5$ ppm for M_1 and $T = 540 \pm 4$ ppm for M_2.

The laser beam is aligned with respect to the cavity by using two steering mirrors m_1 and

Fig. 5. Picture of the optical setup for the cavity prototype at Saclay.

m_2 mounted on tilted stages. Two lenses coated for 1064 nm with focal length $f_1 = -200$ mm and $f_2 = 175$ mm are used to focus the laser beam at the center of the cavity. A Faraday Isolator (Model IO-2.YAG-SP-Z from OFR) protects the Laser from reflected light. The linear polarization of the beam is first rotated with a half-wave plate and then transformed to a circular polarization with a quarter-wave plate. Since the distance between the two mirrors is $L = 80$ cm, the prototype cavity has a g parameter of -0.6, the waist size of the beam at the center of the cavity is $\sigma_{\gamma,0} = 130\,\mu$m, whereas the beam spot on the mirrors is $\sigma_{\gamma,1,2} = 290\,\mu$m (Fig. 7).

The power measured before the beam-splitter cube is 236 ± 12 mW. Taking into account the transmissivity of the cube and the quarter-wave plate, this gives 222 ± 25 mW of light incident on the cavity.

The reflected beam is sent to the photodiode PD_1 using a polarization separator cube. The transmitted beam is split to be analyzed both with the pin photodiode PD_2 and with a CCD camera which allows to view the shape of the beam (Fig. 7). The two photo-diodes are polarized with 18 V and are equipped with a 1064 nm filter. An optical density of 1.3 is placed in front of PD_1 in order to be in the linear regime of the photo-detector.

The optical elements and the laser are mounted on an optical table (Newport, Ref. M-XA-P-44-2) isolated from ground vibration (Newport, Stabilizer: Ref. I-2000-416). The setup is in air and undergoes acoustical vibrations.

5.1.3. Electronics of the feedback loop

Our electronics is composed of two main parts:

- the "discriminator" that generates a DS voltage (upper part of Fig. 8),
- the "filter" or servo controller that must reduce the frequency noise of the system and ensure a convenient loop stability (lower part of Fig. 8).

This system is an adaptation of what was used by the PVLAS experiment [21].

5.1.3.1. The discriminator. For Pound–Drever phase locking, the frequency of the laser is modulated at 680 kHz by applying a sinusoidal voltage of a few mV on the Laser piezoelectric actuator. The image of the reflected intensity of

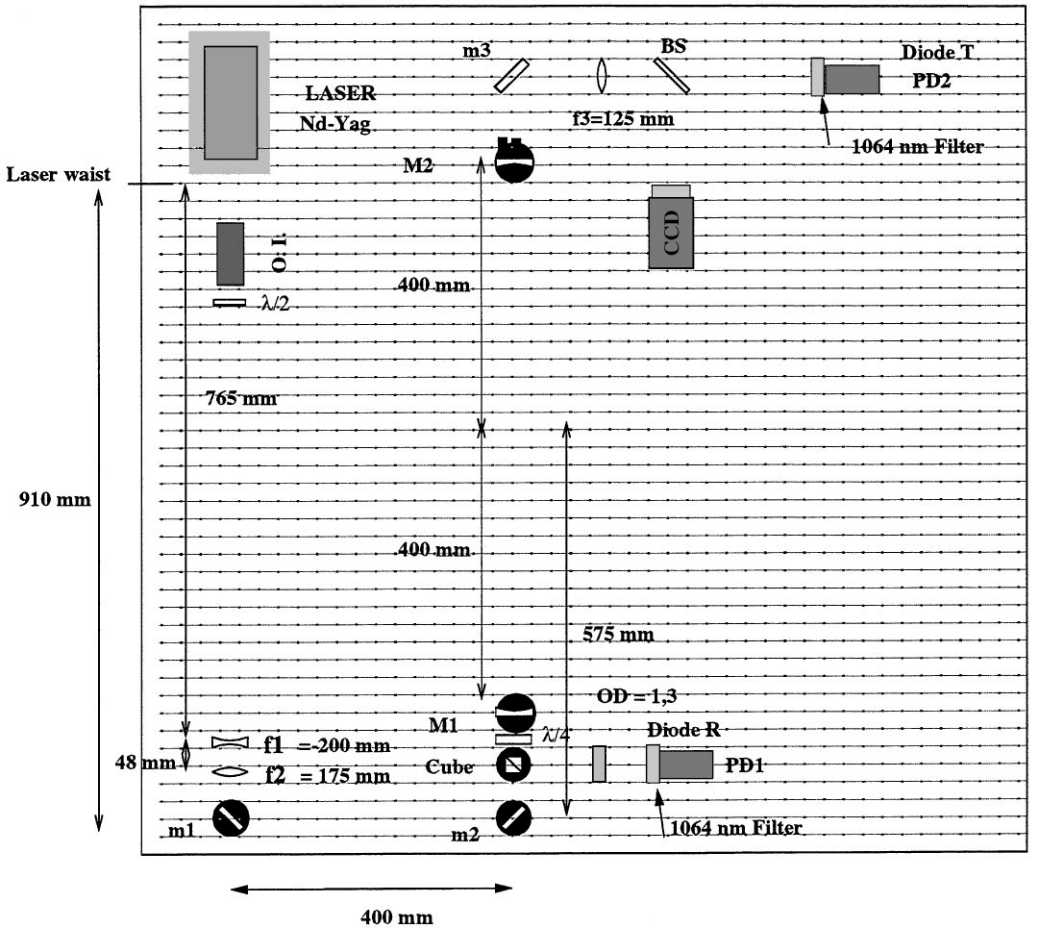

Fig. 6. Optical setup used for the prototype. Elements along the laser path are: a Faraday Optical Isolator (OI), a half-wave plate, two lenses $f_{1,2}$, two steering mirrors $m_{1,2}$, a Beam-splitter Cube, a quarter-wave plate. The Fabry–Pérot cavity (mirrors $M_{1,2}$), a steering mirror m_3, a focalization lens f_3, and a beam-splitter plate.

the laser beam is obtained thanks to a current photodiode signal. There is no photodiode with sensitivity centered at 1064 nm and a high cut-off frequency. Therefore we use a PIN photodiode, Hamamatsu S1223, whose spectral response ranges between 320 nm and 1100 nm. Its cut-off frequency when operating with a reverse voltage of 20 V is 30 MHz. This allows to pass comfortably the useful part of the signal at the modulation frequency.

To transform this photodiode signal into DS, four steps can be distinguished (Fig. 8):

- *Current–voltage conversion*: The photodiode signal is a few mA current, and is turned into a voltage through a 1 kΩ resistor. To improve the stability of the photodiode, the Current–Voltage conversion will be realized by a transimpedance amplifier.
- *Filtering the signal*: In terms of response to optical frequency perturbations $\varepsilon = \varepsilon_0 \sin 2\pi f t$, the Fabry–Pérot cavity is equivalent to a first order filter with a cut-off frequency $f_{\text{cut}} = \Delta\nu_{\text{cav}}/2$. When such a perturbation occurs the reflected light modulated at frequency Ω becomes

$$I_\Omega \propto [\sin(\Omega + 2\pi f)t + \sin(\Omega - 2\pi f)t]\sin\Phi_{\text{R}}. \quad (23)$$

Thus, the useful signal can be found at electronic frequencies $\Omega/(2\pi) - f_{\text{cut}} \leqslant f \leqslant \Omega/(2\pi) + f_{\text{cut}}$.

Table 1
Main characteristics of the optical elements of the prototype (NEW-PORT)

Steering mirrors	m_1, m_2, m_3	Lenses	BK-7 IR coated
Round Pyrex	Ref. 10D20 ER.2	$f_1 = -200$ mm	Ref.KBC031 AR.33
Diameter	25.4 mm	$f_2 = +175$ mm	Ref. KPX103 AR.33
Flatness	$\frac{\lambda_0}{10}$	$f_3 = +125$ mm	Ref. KPX097 AR.33
Loss	5%[a]	diameter	25.4 mm
		Loss	1%[a]
Polarization	IR coated	Beam-splitters	IR coated
$\frac{\lambda}{4}$	Ref. 10RP04-34	Cube	Ref. 10BC16 PC.9
Transmissivity	$T = 99.75\%$[a]	Extinction ratio	$> 500:1$
$\frac{\lambda}{2}$	Ref. 10RP02-34	Transmissivity	$T > 95\%$
Transmissivity	$T = 99.75\%$[a]	Plate	Ref. 10B20NC.3
		Transmissivity	$T = 93.4\%$[a]

[a]Measured.

Using a band pass filter adapted to this range would improve the signal to noise ratio. We are currently using a bandpass filter between [300 Hz, 1.6 MHz].

- *Demodulation*: The modulated signal coming from the band pass filter is mixed with a signal whose frequency is equal to the modulation frequency $\Omega/(2\pi)$. We are using at present a ring mixer *ZP*10514 from *Mini-Circuit*.
- *Amplification*: To optimize the error signal (a few mV after demodulation), an inverter amplifier (static gain 60, cut-off frequency $f_2 \simeq 300$ kHz) is used to adapt its amplitude to the full scale (10 V) of the voltage range.

The transfer function of the discriminator D_V can thus be summarized by its static gain $D_V^0 \simeq 0.45\,\mathrm{V\,kHz^{-1}}$ (this is the slope of the DS for zero detuning, Fig. 11), and two cut-off frequencies $f_1 = \Delta\nu_{cav}/2$ and f_2, the cut-off frequency of the inverter amplifier.

5.1.3.2. The filter. For the servo (Fig. 8), four analogic integrators are used for each channel (FAST and SLOW actuators). The first three stages are common to both channels. They can be switched independently to analogic amplifiers to study feedback stability and noise reduction.

To model the noise reduction achieved by the feedback loop, we use a block diagram (Fig. 9), where each optical and electronic device is replaced by a block associated with its transfer function. Three sources of noise defined by their spectral density have been considered: the laser and cavity noise S_L ($\mathrm{Hz\,Hz^{-1/2}}$), the electronic noise S_{servo} ($\mathrm{V\,Hz^{-1/2}}$) and the discriminator noise S_{discri} ($\mathrm{V\,Hz^{-1/2}}$). The noise we have to reduce is the optical noise S_L, but the feed-back can also reduce the other noises. At low frequency the $1/f$ noise dominates and at higher frequency the white noise dominates.

As already stated, as frequencies above the cavity cut-off frequency, the cavity itself reduces the noise. The noise reduction in the medium frequency range, $0.1\,\mathrm{Hz} \leqslant f \leqslant f_{cut}$, is performed by the FAST channel. For the FAST channel, the spectral density of the noise of the system (i.e. of the frequency difference between the laser and a resonance of the cavity) in closed loop $S_{L,cl}$ is given by

$$S_{L,cl} = \frac{\sqrt{S_L^2 + |K_F S_{servo}|^2 + |K_F\ G_F S_{discri}|^2}}{|1 + K_F G_F D_V|} \simeq \frac{S_{discri}}{|D_V\ |}, \tag{24}$$

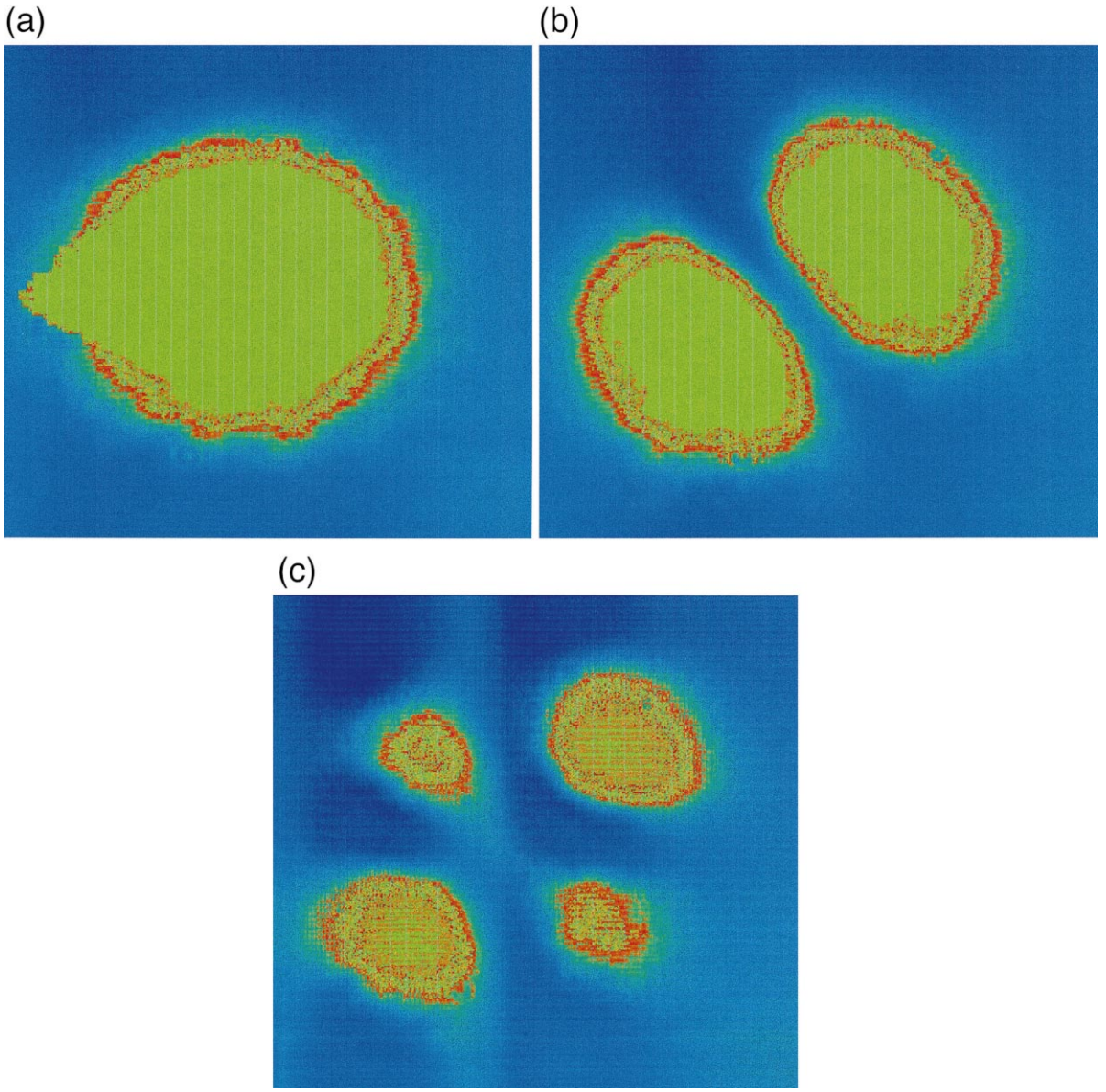

Fig. 7. Transverse mode (TEM_{00}, TEM_{10} and TEM_{11}) at the exit of the cavity as seen by the CCD camera (scale roughly 1 mm $\times$ 1 mm).

where the approximation holds for very large values of the servo gain G_F. Thus working with large servo gains ends up reducing all the noises, but the discriminator. The servo used for the results presented in this paper (Fig. 8), has a gain of 280 dB at 1 Hz and reaches 0 dB at 5 kHz (Fig. 9).

At low frequencies ($f \simeq 1$ Hz) mechanical perturbations of the cavity and slow drift of the Laser could result in large change ($\simeq$ GHz) of the detuning. This could not be corrected by the FAST actuator because of its reduced tuning coefficient ($K_F \simeq 3\,\mathrm{MHz\,V^{-1}}$), and the SLOW actuator has to

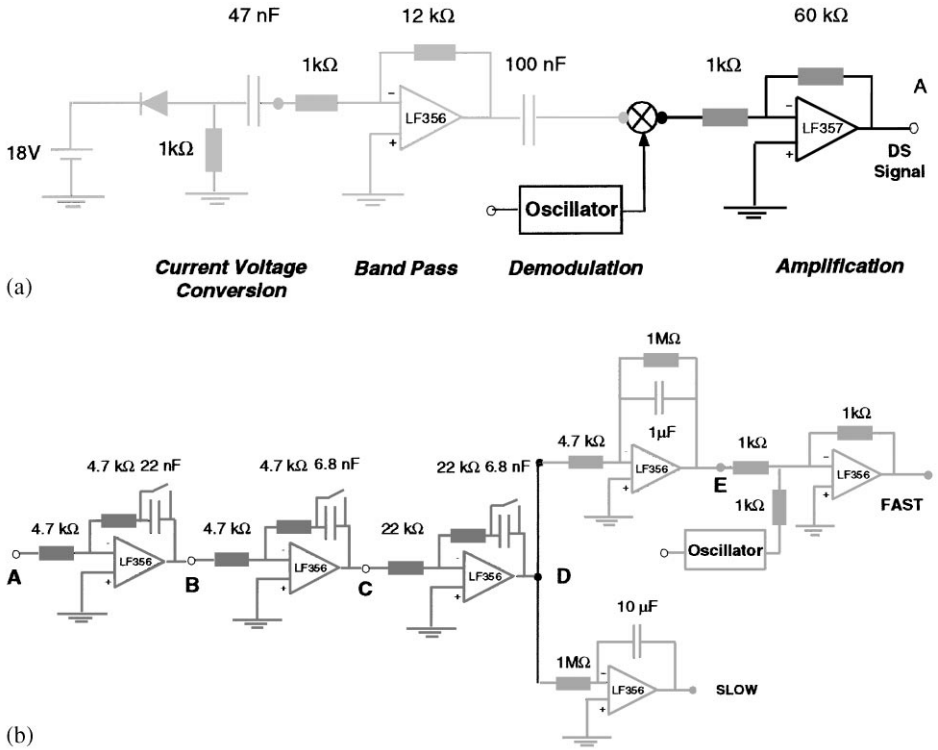

Fig. 8. Photodiode and Servo electronics. Three integration stages (AB, BC, CD) are common to the FAST and SLOW actuators. Amplifiers are from National Semiconductor.

be used. In practice, this is done by assuring that at low frequency the gain of the SLOW servo is higher than the gain of the FAST servo.

For the first three stages, resistors and capacitors values are determined to achieve the optimal value of the gain, resulting from a compromise between noise reduction and loop stability. For the fourth stage, resistors and capacitors values are determined to adapt the desired frequency range of each channel.

To ensure a good loop stability it is necessary for an unity open loop gain to have a phase rotation far from $(2k+1)\pi$. This unity gain is centered around the cavity cutoff frequency. For a first order transfer function and frequencies higher than the cutoff frequency the slope is equal to -20 dB/decade which means a phase rotation of $\pi/2$. These phase rotations in the loop are equal to $\pi/2$ for the actuator K_F or the fast integrator, π for D_V (due to the cavity and the amplifier). The loop phase rotation is then equal to 2π which gives a good stability but not the best step response. The improvement of the cavity, the use of a faster amplifier and the modification of the fast integrator transfer function will give a phase rotation around $\pi/2$ ensuring a good stability and an efficient step response.

Two difficulties are very disturbing for system modeling and optimization:

- the transfer function of the FAST servo frequency tuning coefficient (K_F) is hardly known,
- the cavity cut-off frequency is too close to the supposed K_F cut-off frequency.

With such difficulties it is very hard to determine Phase Margin and noise reduction with a good accuracy.

A higher finesse cavity should solve this problem but needs a complex filter design.

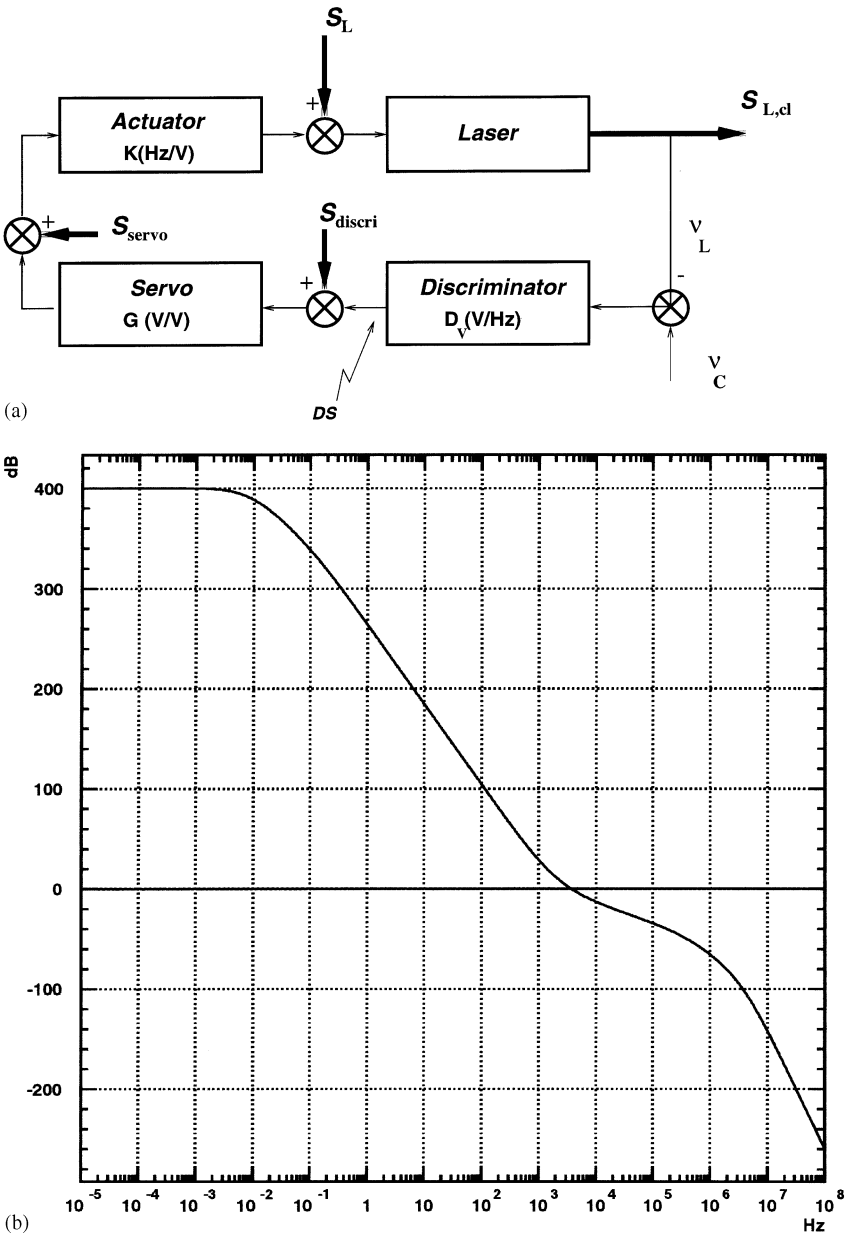

Fig. 9. Top: Block Diagram for noise modeling in the feedback loop. The actuator and servo transfer functions for the FAST (resp. SLOW) channel are $K = K_F$ and $G = G_F$ (resp. $K = K_S$ and $G = G_S$). Bottom: Transfer function for the Fast channel.

5.2. Results

A CCD view of the cavity when the Laser is locked is given in Fig. 10.

The cavity bandwidth has been measured by recording the transmitted beam intensity as a function of time when ramping the laser frequency, with open feedback loop (Fig. 11). The small peaks on

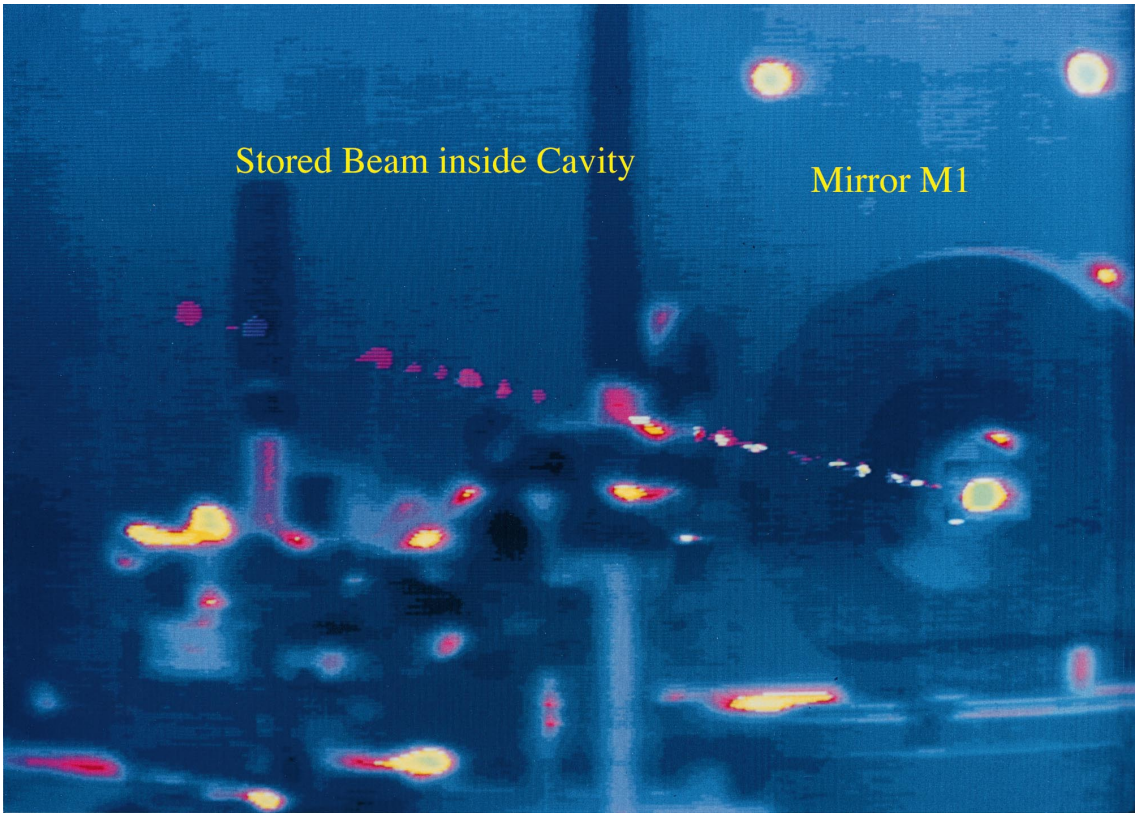

Fig. 10. CCD view of the Fabry–Pérot cavity: 15 s Recording time.

the sides are due to the laser modulation and are separated by twice the modulation frequency. (This gives the scale between the times and the optical frequency). The measured FWHM is $\Delta\nu_{cav} \simeq 112 \pm 5$ kHz. The finesse $\mathscr{F}$ of the cavity is thus $\mathscr{F} = \Delta\nu_{FSR}/\Delta\nu_{cav} \simeq 1670 \pm 75$. In the framework of the use of a Fabry–Pérot cavity for Compton Polarimetry, the relevant parameters are the photon density inside the optical cavity, the beam stability and the reliability of the system. Up to now, the reliability of our system is given by the time during which the system is under feedback control, i.e. with power inside the cavity. This time is now up to two hours when the cavity is protected against dust.

The beam intensity inside the cavity I_{cavity} is monitored using the PD_2 calibrated photodiode. The absolute value is determined by $I_{cavity} = I_{PD_2}/T_{M_2}T_o$, where I_{PD_2} is the intensity measured by the PD_2 photodiode, T_{M_2} the transmissivity coefficient of the M_2 mirror of the cavity and T_o the transmissivity coefficient of the optical element located between M_2 and the photodiode. With the described cavity, we found $I_{cavity} \simeq 40 \pm 4$ W.

To evaluate the performance of the servo, the spectral density of the DS voltage has been recorded using a spectral analyser HP 89410 A with and without the 3 integrators (Fig. 12). The low-frequency noise drops from -60 db (140 Hz $Hz^{-1/2}$) to -100 dB (1.4 Hz $Hz^{-1/2}$) when the servo operates with the 3 integrators. Another useful measurement is the time evolution of the power stored in the cavity. In order to study the medium and high frequency domain of this time evolution, the noise spectral density of the transmitted light monitored with the PD_2 photodiode

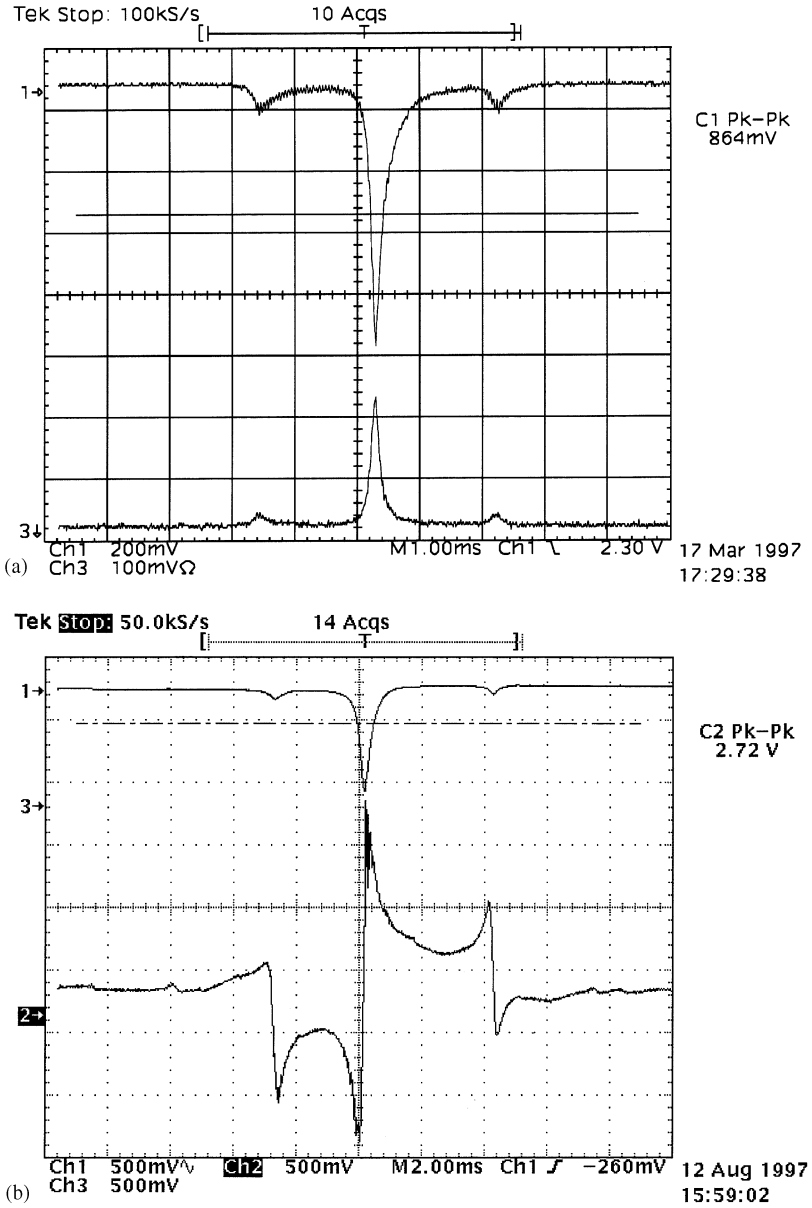

Fig. 11. Top: Reflected and transmitted light by the cavity as measured by the two photo-diodes, when slowly (10 V_{pp} at 5 Hz) ramping the laser frequency. The side bands are separated by $2\nu_{\Omega}$. Bottom:DS signal, after the amplification stage.

was recorded. The corresponding DC level of the photodiode output was 2.3 V. As can be computed from Fig. 12, the RMS noise for frequencies above 60 Hz is typically 6 mV, (less than 0.3%). At Lower frequency the noise increases to 20 mV, (i.e. 0.9%) for frequencies above 1 Hz. In order to estimate the noise of the system at lower frequencies, the PD_2 photodiode voltage was sampled at 4 Hz with

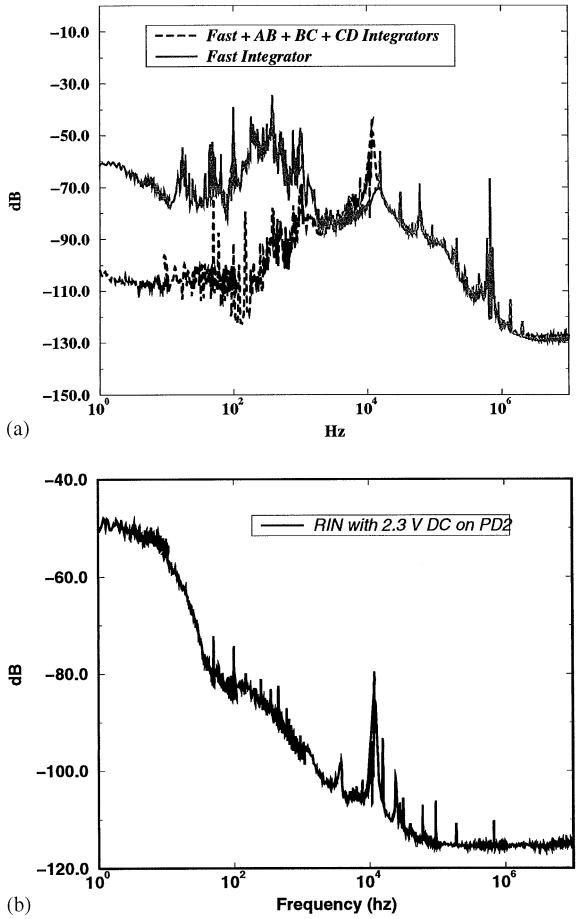

Fig. 12. Spectral density for the DS, measured after the gain 60 for a DC voltage of 2.3 V and Relative Intensity Noise of the beam transmitted by the cavity. Measured with an HP 89410A Vector signal analyzer (1 V reference level).

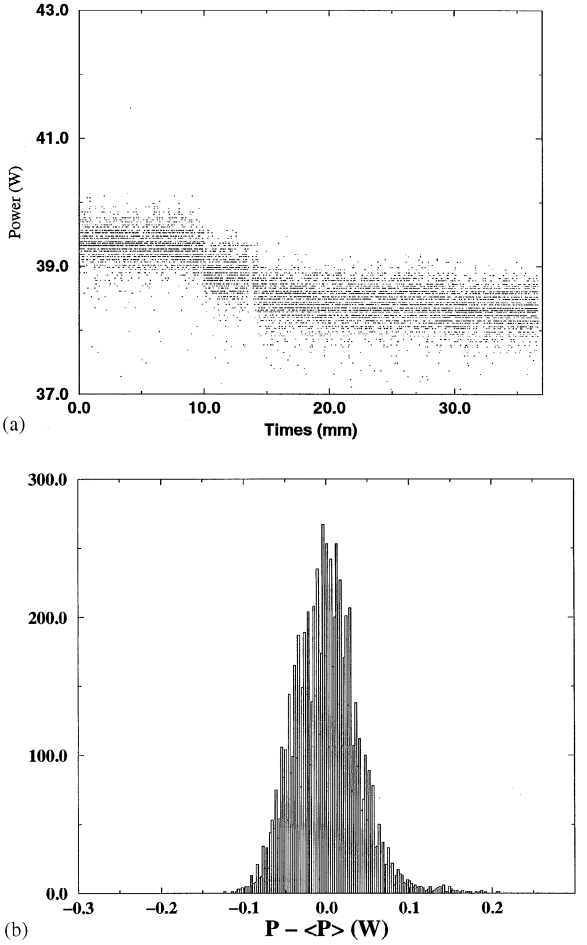

Fig. 13. Intra-cavity intensity as a function of the time, showing a RMS dispersion close to 1% after slow drift subtraction.

a VME acquisition system to monitor the beam stability. The beam stability $\Delta I/I$ over 30 min period is close to 1% RMS (Fig. 13).

6. Conclusion and outlook

A prototype of a Fabry–Pérot Cavity for Compton Polarimetry has been operated successfully, giving a photon power density (at $\pm 1\sigma$) of $30\,\mathrm{kW\,cm^{-2}}$. In standard TJNAF conditions, this would allow a measurement of the electron beam polarization at the 1% statistical level within 3 h.

The next step will be to install such a cavity on the TJNAF electron beam. As a conclusion, the various difficulties expected in this process are reviewed.

In order to maximize the luminosity, a crossing angle of 20 mrad is foreseen. For a 1 m cavity (the maximum possible length taking into account the space available on the Hall A TJNAF beam line (Fig. 6)), and with very small mirrors (1/4 in.), this corresponds to mirrors approaching the electron beam at 5 mm. The consequence is that the mirrors will have to be in vacuum, resulting in a more difficult alignment of the optical cavity. Two

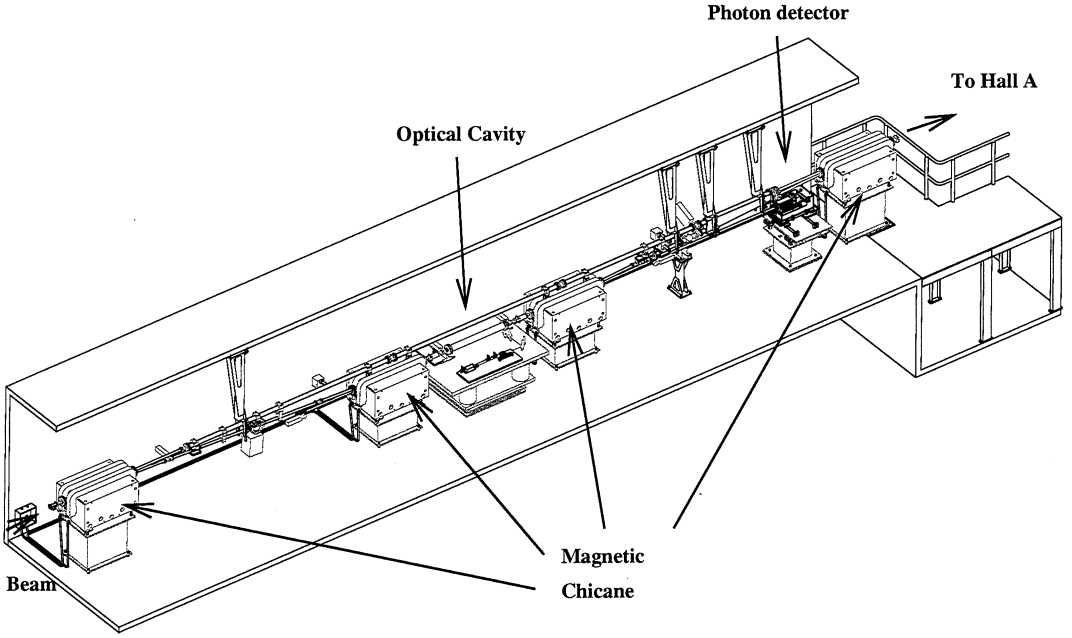

Fig. 14. The Compton Polarimeter Setup at TJNAF Hall A. Total length 15 m.

solutions are possible:

- *Movable mirrors*: Mount the mirrors on piezoelectric (remotely controlled) actuators in vacuum.
- *Monolithic cavity*: The mirrors are fixed on the walls of the cavity vacuum chamber. This requires that the vacuum chamber of the cavity has a very precise mechanical definition to ensure that the Fabry–Pérot cavity will be resonant in the fundamental mode.

We are currently working on the design of a 80 cm monolithic cavity prototype with $g = -0.7$, mechanical tolerances of ± 0.65 mm and for which diffraction losses are small.

An other concern about running a Fabry–Pérot cavity on an accelerator is radiation damage. All optical elements, especially the Laser itself, will be shielded when possible. Unfortunately, shielding of the cavity mirrors is difficult. Some data exist on the radiation damage to Ta_2O_5/SiO_2 multi-layer mirrors [22,23], but they are difficult to extrapolate for TJNAF conditions, making a measurement of mirror degradation mandatory.

The following step in the design of the Compton Polarimeter cavity (Fig. 14) is to work with a high Finesse cavity, e.g. to use high-quality mirrors. Super-Mirrors available from industry [25] have now good reflectivity ($R \simeq 99.97\%$), low transmissivity ($T \simeq 0.12\%$), and reasonable losses $P \leqslant 100$ ppm. One can thus expect to reach a finesse of $\mathscr{F} \simeq 10\,000$, and a gain of $\mathscr{G}_0 \simeq 2000$. This could be acceptable for our cavity, unfortunately these Super-Mirrors are limited by the maximum power density tolerated ($1\,\mathrm{kW\,cm^{-2}}$). For a 0.5 W Laser, trapped in a 1 m cavity with $g = -0.95$, i.e. a beam diameter on the mirrors close to 1 mm, with a gain of $\mathscr{G}_0 = 2000$ (resp. $\mathscr{G}_0 = 10\,000$), the power density is $100\,\mathrm{kW\,cm^{-2}}$ (resp. $500\,\mathrm{kW\,cm^{-2}}$). Such a power density is not available from industry yet, that's why, our final mirrors will be built by the VIRGO collaboration [24].

The mirrors have the structure $LL(HL)_N HS$ where L (resp. H) stands for a $\lambda/4$ layer of low (resp. high) index material and S for the substrate. They are made of Ta_2O_5 layers with High index $n \simeq 2.1$, and SiO_2 with low index $n \simeq 1.47$ deposited on

a super polished silica substrate using the technology of Ion beam sputtering. To minimize the loss due to scattering, the layers are made of amorphous deposit. The mirror reflectivity is governed by the design of the layers. We will use $(HL)_{14}$ mirrors with transmissivity $T = 1 - R - P \simeq 100$ ppm, scattering and absorption loss $P \simeq 5$ ppm. We thus expect a maximum cavity gain $\mathscr{G}_0 \simeq 9070$ at 1064 nm.

References

[1] L. Cardman, Nucl. Phys. News 6 (4) (1996) 18.
[2] B. Wagner et al., Nucl. Instr. and Meth. A 294 (1990) 541.
[3] K.B. Beard et al., Nucl. Instr. and Meth. A 361 (1995) 46.
[4] D. Gustafson et al., Nucl. Instr. and Meth. 165 (1979) 177.
[5] D.P. Barber et al., Phys. Lett. 135B (1984) 498.
[6] M. Placidi, R. Rossmanith, Nucl. Instr. and Meth. A 274 (1989) 79.
[7] D.P. Barber et al., Nucl. Instr. and Meth. A 329 (1993) 79.
[8] M. Woods, The scanning Compton polarimeter for the SLD experiment, in: SPIN'96, Amsterdam, Netherlands, 9 September 1996, pp. 843–845.
[9] G. Shapiro et al., SLAC-PUB-6261, 1993.
[10] C. Prescott, SLAC Internal Report, SLAC TN 73 1.
[11] A. Denner, S. Dittmaier, Nucl. Phys. B 407 (1993) 43.
[12] E. Beise et al., Measurements of strange quark effects using parity-violating elastic scattering from ^{4}He at $Q^2 = 0.6$ $(GeV)^2$, Jefferson Lab. Experiment E-91-004, 19XX.
[13] P. Souder et al., Parity violation in elastic scattering from the proton and ^{4}He, Jefferson Lab. Experiment E-91-010.
[14] P.W. Milonni, J.H. Eberly, Lasers Willey-Inter-science, New York, 19XX.
[15] A. Siegman, Lasers, University Science Book, Mill Valley, CA, 1986.
[16] M. Born, E. Wolf, Principles of Optics, Pergamon Press, Oxford, 1975.
[17] R.W.P. Drever et al., Appl. Phys. B 31 (1983) 97.
[18] N.M. Sampas Thesis, Colorado University, 1990, unpublished.
[19] T. Day, Thesis, Stanford University, 1990, unpublished.
[20] G. Cantatore et al. Rev. Sci. Instr. 66(4) (1995).
[21] Guido Zavattini et al., Rev. Sci. Instr. 66 (1995) 2785; P. Pace, Tesi di Laurea in Fisica (1993–94), Trieste University, unpublished; G. Ruoso, Tesi di Dottorato in Fisica (1993–94), Padova University, unpublished.
[22] M.E. Couprie et al., Proc. Int. Symp. of Optical Interference Coating, Grenoble, 1994.
[23] M.E. Couprie et al., Appl. Opt. 30 (1991) 344.
[24] C. Bradaschia et al., The VIRGO project, Nucl. Instr. and Meth. A 289 (1990) 519.
[25] Micro-controle Catalogue, 1994, p. 7.16.